Journal of Cellular Biochemistry 57:557–573 (1995)

Properties of Blood-Contacting Surfaces of Clinically Implanted Cardiac Assist Devices: Gene Expression, Matrix Composition, and Ultrastructural Characterization of Cellular Linings

Michael J. Menconi, Shirwin Pockwinse, Thomas A. Owen, Kurt A. Dasse, Gary S. Stein, and Jane B. Lian

Department of Cell Biology, University of Massachusetts Medical School, Worcester, Massachusetts 01655-0106 (M.J.M., S.P., T.A.O., G.S.S., J.B.L.); Thermo Cardiosystems, Woburn, Massachusetts 01888-1799 (K.A.D.)

Abstract The development of implantable cardiac assist devices for prolonged circulatory support has been impeded by the problem of excessive thrombogenesis on the blood–prosthetic interface, with subsequent embolization. To overcome this obstacle, a ventricular assist device has been developed with textured blood-contacting surfaces to encourage the formation of a tightly adherent, hemocompatible, biological lining. In this study, we applied molecular biological techniques, in conjunction with conventional ultrastructural and biochemical techniques, to characterize the biological linings associated with the blood-contacting surfaces of 11 of these devices, which had been clinically implanted for durations ranging from 21 to 324 days. No clinical thromboembolic events or pump-related thromboembolism occurred. Biological linings developed on the textured surfaces composed of patches of cellular tissue intermingled with areas of compact fibrinous material. In addition, islands of collagenous tissue containing fibroblast-like cells appeared after 30 days of implantation. Many of these cells contained microfilaments with dense bodies indicative of myofibroblasts. RNA hybridization analyses demonstrated that the colonizing cells actively expressed genes encoding proteins for cell proliferation (histones), adhesion (fibronectin), cytoskeleton (actin, vimentin) and extracellular matrix (types I and III collagen). Linings, which never exceeded 150 μm in thickness, remained free of pathological calcification. Textured blood-contacting surfaces induced the formation of a thin, tightly adherent, viable lining which exhibited excellent long-term hemocompatibility.

Key words: cardiac assist device, pseudointima, hemocompatibility, polyurethanes, myofibroblast

Over the past 30 years, a number of mechanical circulatory support systems, such as total artificial hearts and ventricular assist devices, have been developed to treat patients with end-stage cardiac disease. The majority of these devices were designed to have smooth blood-contacting surfaces, primarily consisting of elastomeric biomaterials, as a means of successfully preventing thrombogenesis [1,2]. However, despite advances in the management of patients with anticoagulants and antiplatelet therapy, as well as improvements in the design and selection of biomaterials [3,4], thrombogenesis on smooth blood-contacting surfaces with subsequent thromboembolic complications persist as significant problems in the clinical applications of these devices [5–7].

An alternative approach for controlling thromboembolic events involves utilizing biomaterials fabricated with textured blood-contacting surfaces [8,9]. Textured biomaterial surfaces are designed to encourage the formation and adherence of a stable, hemocompatible, biological lining derived from circulating blood elements. Ideally, the resultant lining masks the underlying biomaterial surfaces and mimics the function of the natural endothelium in preventing thrombogenesis. Preliminary studies conducted in animal models demonstrated that textured blood-contacting surfaces promote the formation of a well-adherent, hemocompatible, biological lining [10,11]. Initially, the deposition of circulating blood elements occurs, forming a fibrin-cellular coagulum. This initial lining gradually

Abbreviations used: LVAD, left ventricular assist device.

Received July 25, 1994; accepted August 29, 1994.

Address reprint requests to Dr. Jane B. Lian, Department of Cell Biology, University of Massachusetts Medical School, 55 Lake Avenue North, Worcester, MA 01655.

reorganizes with the colonizing cells eventually producing a collagenous matrix. However, long term bovine studies have revealed that these blood-derived linings, although tightly adherent, increase in thickness over time and frequently undergo extensive calcification, events which ultimately result in device failure [12–14].

Recent technological advances in the fabrication of textured blood-contacting surfaces have lead to the development of a totally implantable left ventricular assist device (LVAD) for use in permanent, long-term support in patients with irreversible cardiac dysfunctions. Currently, a pneumatically driven version of the system has been approved by the U.S. Food and Drug Administration (FDA) for investigational clinical use as a bridge to cardiac transplantation. Thus far, the LVAD has been used in 106 clinical cases for periods up to 324 days, with 69% of the bridge to transplant patients having undergone transplantation, and 85% of these individuals remaining alive up to 28 months following transplantation. Preliminary clinical studies have demonstrated that a thin, cellular, hemocompatible lining develops on the blood-contacting surfaces of this device after short-term (<6 weeks) implantation [15].

In the present study, explants from eleven patients, who were supported with these texture-surfaced LVADs for periods ranging from 21 to 324 days, were examined. A molecular biological approach, in conjunction with ultrastructural and biochemical techniques, was used to characterize the cells and matrices comprising the biological linings associated with the blood contacting surfaces as a function of implant duration. Our analyses indicate that these colonizing cells can maintain a thin, tightly adherent, hemocompatible lining with only minimal anticoagulation therapy. This study represents the first evaluation of the long-term performance of textured blood-contacting surfaces in humans.

MATERIALS AND METHODS

Device Description

The Heartmate-1000 LVAD, developed and manufactured by Thermo Cardiosystems Inc. (Woburn, MA), is an implantable, pneumatically driven pusher-plate type blood pump composed of an outer rigid titanium housing and a flexible polyurethane diaphragm. As shown schematically in Figure 1, the pump is positioned intraperitoneally in the left upper quadrant of the

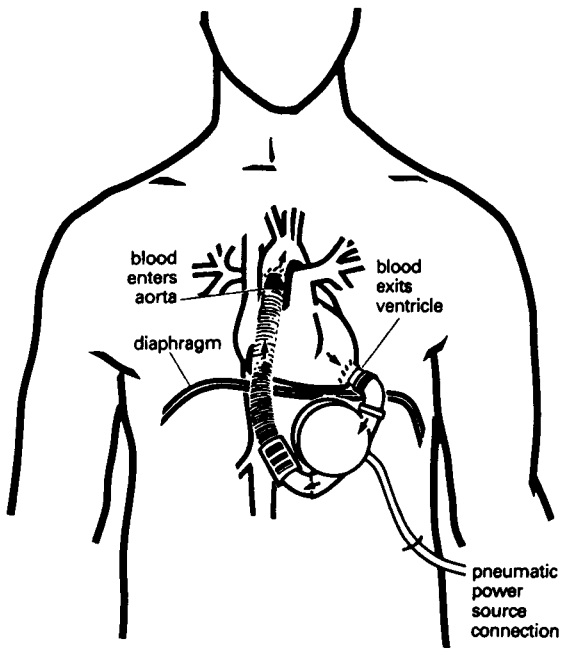

Fig. 1. Schematic illustration of the LVAD implanted in patient. The pump is positioned intraperitoneally in the upper left quadrant of the abdomen. Dacron conduits are used to connect the pump between the apex of the left ventricle and the ascending thoracic aorta. The LVAD is pneumatically driven via a percutaneous drive line powered by an external console. Porcine valves placed in the inflow and outflow conduits ensure the unidirectional flow of blood (*arrows*).

patient's abdomen and, when implanted for temporary use, is powered by an external console. Low-porosity Dacron conduits connect the pump between the apex of the left ventricle and the ascending thoracic aorta. Programmed pulses of pressurized air are delivered to the implanted pump chamber via a percutaneous drive line that penetrates the body through a subcostal incision. When the pulse pressure is increased, the pusher plate is displaced towards the pump housing, and the blood is expelled from the pump into the ascending aorta. Between the pressure pulses, the pump refills by drawing blood from the left ventricle. The inflow and outflow conduits of the device contain 25-mm porcine xenograft valves (Medtronic Blood Systems, Irvine, CA) to ensure the unidirectional flow of blood. The LVAD has a maximum pump stroke volume of 83 ml/beat and is capable of providing blood flows in excess of 10 L/min.

The blood contacting surfaces of both the titanium housing component and the flexible polyurethane diaphragm are textured (Fig. 2) to encourage the formation and adherence of a biologic lining. The flexible diaphragm consists

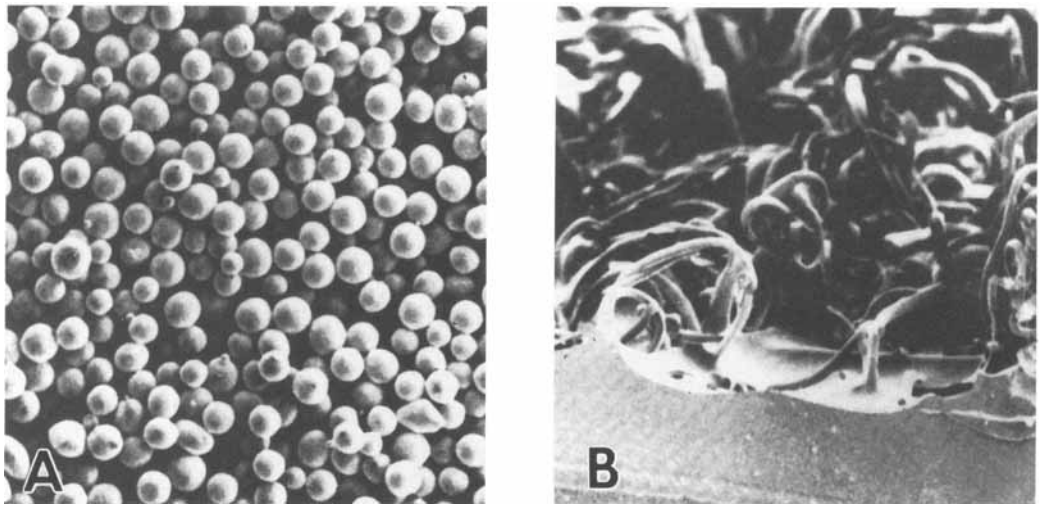

Fig. 2. Topography of the textured blood-contacting surfaces used in the Heartmate-1,000 LVAD. **A:** Sintered titanium microsphere surface of the rigid housing (×50). **B:** Integrally textured polyurethane fibrillar surface of the flexible diaphragm (×100).

of a fibrillar surface integral with the base material to eliminate detaching of the fibrils. The individual fibrils measure approximately 18 μm in diameter and 300 μm in length. The nonflexing housing surface is fabricated from titanium microspheres sintered together to form a porous nonpermeable topography. The diameter of the spheres ranges from 50 to 75 μm, with a resultant pore size ranging from 25 to 50 μm.

Sample Retrieval Protocol

For most supported patients, the LVADs were retrieved immediately after the pneumatic drive consoles were turned off. However, in the case of patients supported for 114, 189, and 233 days, the drive consoles were turned off and the devices were left remaining in the patient, without blood circulating through the pumps, for 32.5, 3.5, and 33 h, respectively, before actual retrieval (staged explantations).

Each blood pump was processed in precisely the same manner at the time of explant. After removal from the patient, the pump chamber was carefully opened, rinsed in buffered saline and photographed. The integrally textured polyurethane diaphragm was then removed from the pusher plate and divided in half between the inflow and outflow regions of the pump chamber. The inflow half was fixed in 2% paraformaldehyde in 0.1 M cacodylate buffer (pH 7.5) for 15 min and then stored in 0.1 M cacodylate buffer (pH 7.5) for morphological analysis. The outflow half was immediately frozen in liquid nitrogen

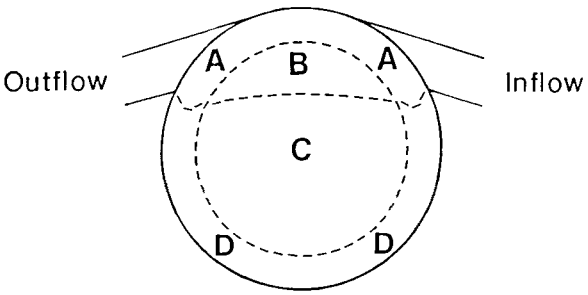

Fig. 3. Hemodynamic conditions and mechanical flexure patterns within the LVAD pumping chamber. **A:** High-shear/high-flex region. **B:** High-shear/low-flex region. **C:** Low-shear/low-flex region. **D:** Low-shear/high-flex region.

for biochemical evaluations. Likewise, after selected samples from the titanium microsphere surface were fixed in paraformaldehyde, the entire housing was rapidly frozen in liquid nitrogen. The time interval from explantation to freezing averaged approximately 30 min.

For morphological and biochemical evaluation, diaphragm samples were analyzed from regions exposed to various combinations of diaphragm flexure patterns and blood flow conditions, which vary in a complex manner depending on the geographic location within the pump chamber. As schematically illustrated in Figure 3, the greatest shear rates of blood along the walls of the device are found in the region between the inflow and outflow ports (regions A and B). Flexure of the diaphragm is uniformly high around the circumference of the diaphragm (i.e., regions A and D), but very low within the

central area bonded to the pusher plate. This central region (region C) is exposed to the lowest combination of shear rates and diaphragm flexure. The sampling of diaphragm regions was selected to permit possible correlations of morphologic and biochemical findings with the hemodynamic conditions and mechanical flexure patterns existing within the pump chamber.

Scanning Electron Microscopy

Samples were postfixed in 1% osmium tetroxide in 0.1 M cacodylate buffer (pH 7.5) for 15 min at room temperature, dehydrated in a graded series of increasing concentrations of ethanol (70%, 80%, 95%, 100%), and allowed to air dry from 100% ethanol. The samples were subsequently sputter-coated with gold to a thickness of 5 nm and examined on a Jeol JSM-35 at an accelerating voltage of 25 kV.

Transmission Electron Microscopy

Samples were postfixed in 1% osmium tetroxide (in 0.1 M cacodylate buffer, pH 7.5), dehydrated, and embedded in Poly/Bed 812 (Polysciences, Warrington, PA). After sectioning, specimens were stained with 4% uranyl acetate and Reynolds' lead citrate and examined under a Philips 400T transmission electron microscope.

Energy-Dispersive X-Ray Spectroscopy

For EDS analysis, samples were fixed and dehydrated as described for SEM. The samples were then carbon coated and examined for possible pathological calcification on a Joel JSM-6100 at an accelerating voltage of 10 kV.

Histology

Samples for light microscopy were dehydrated as described for SEM, embedded in JB-4 methacrylate resin (Polysciences, Warrington, PA), and sectioned to a thickness of approximately 5 microns. Staining was performed with hematoxylin & eosin (H&E) for overall cellular morphology. Toluidine blue (0.5%) distinguished acidic connective tissue matrices. To examine for the presence of muscle fibers with collagen, trichrome staining was performed using a modification of the Osheroff-Ruffing procedure [16].

Total Collagen and Protein Measurements

Approximately 1–2-cm^2 sections of the fresh frozen diaphragms were incubated in 1.0 ml 6N Ultrex HCl for 5 h at 37°C. After sonication followed by vigorous mechanical pipetting to dislodge the tissue linings completely from the diaphragm sections, the HCl solutions were transferred into Pyrex tubes; the samples were hydrolyzed at 110°C for 24 h under vacuum after flushing with N_2. Hydrolyzates were dried under N_2, reconstituted in 0.01N HCl, and then subjected to amino acid analysis on a Beckman 121 M automated analyzer. Total collagen content was estimated by determining the residues of hydroxyproline/1,000 residues of all amino acids, assuming that hydroxyproline comprised 10% of the total number of amino acid residues found in collagen [17].

RNA Isolation and Analysis

For isolating total cellular RNA, the tissue linings were solubilized from the titanium housing and polyurethane diaphragm surfaces using a lysis buffer composed of 1.4 mM Tris–HCl, 0.7 mM EDTA, 2.6% SDS, 100 μg/ml proteinase K (Boehringer Mannheim, Indianopolis, IN), and 10 μg/ml polyvinylsulfuric acid, pH 7.4. The samples, which were extremely viscous, were briefly sonicated to disperse the tissue and incubated for 30 min at room temperature on a shaker. The nucleic acids in the samples were extracted with equal volumes of phenol and chloroform/isoamyl alcohol (24:1), precipitated with 3 vol of 95% ethanol at −20°C overnite and recovered by centrifugation. To digest the DNA from the samples, the pellets were incubated with RQ1 DNase I (Promega Corp., Madison, WI) at a concentration of 20 U/sample in a reaction volume of 400 μl for 20 min at 37°C. After extracting the RNA from the samples with phenol and chloroform/isoamyl alcohol, the RNA was reprecipitated with 95% ethanol at −70°C, recovered by centrifugation and stored at −70°C.

All RNA preparations were quantitated by absorbance measurements at 260 nm. The intactness of the RNAs was evaluated by ethidium bromide staining following electrophoresis in 6.6% formaldehyde–1% agarose gels. RNA samples were directly applied to Zeta-Probe blotting membranes (BioRad, Richmond, CA) using a Minifold II Slot Blot System under conditions described by the apparatus manufacturer (Schleicher and Schuell, Keene, NH).

RNA samples were hybridized with the following cDNA probes: rat H_4 histone [18]; human β-actin [19]; human vimentin [20]; rat fibronectin [21]; rat Type I collagen [22]; bovine Type III collagen [23]. All DNA probes were labeled with

TABLE I. Summary of Clinical Implants

Patient code	Age/sex	Diagnosis	LVAD support (days)	Outcome
WHC-01	57/M	MI	21	TP/alive
WHC-02	47/M	MI	23	WEANED/EXP
THI-15	41/M	IDIO-CMP	31	TP/alive
THI-09	22/M	IDIO-CMP	35	TP/alive
THI-07	48/M	IDIO-CMP	37	TP/alive
THI-11	52/M	ISCH-CMP	84	TP/alive
THI-12	43/M	IDIO-CMP	114	TP/alive
THI-10	39/M	ISCH-CMP	132	TP/alive
THI-14	55/M	IDIO-CMP	189	TP/alive
THI-13	42/M	IDIO-CMP	233	TP/alive
CPM-01	35/F	VIR-CMP	324	TP/alive

MI, myocardial infarction; IDIO, idiopathic; ISCH, ischemic; VIR, viral; CMP, cardiomyopathy; TP, transplanted; EXP, expired.

^{32}P-dCTP by the random primer method [24] to a specific activity of at least 1×10^9 dpm/μg DNA. All prehybridizations and hybridizations were performed in 50 mM $NaPO_4$ buffer (pH 6.5) containing 50% formamide, 5× SSC (0.75 M NaCl, 75 mM sodium citrate), Denhardt's solution (0.1% Ficoll, 0.1% polyvinyl pyrrolidone), 1% sodium dodecyl sulfate (SDS), and 250 μg/ml salmon sperm DNA at 42°C for 18 h. For hybridization, 10^6 cpm/ml probe and 10% dextran sulfate were added [25]. Following hybridization, the blots were washed twice at room temperature in 2× SSC/0.1% SDS (30 min per wash) and then once at 65°C in 1× SSC/0.1% SDS (30 min) for nonhomologous probes or an additional two times in 0.2× SSC/0.1% SDS at 65°C for homologous probes (30 min per wash). Blots were then exposed to XAR-5 X-ray film (Kodak) using a Cronex Lightning Plus Screen at −70°C. Relative intensities of bands on the autoradiograms were quantitated by scanning laser densitometry (LKB 2400 GelScan XL) within the linear range of signals. Data are expressed in densitometric units.

RESULTS

Clinical Evaluation

As summarized in Table I, patients supported with the Heartmate LVAD ranged from 22 to 57 years of age and were admitted with diagnoses of acute myocardial infarction (2 patients), idiopathic cardiomyopathy (6 patients), viral cardiomyopathy (1 patient), and ischemic cardiomyopathy (2 patients). Ten of the 11 patients, whose conditions were classified as irreversible, ultimately underwent cardiac transplantation, whereas one patient (WHC-02), who was diagnosed with a reversible heart condition, was eventually weaned off the device. Before LVAD implantation, all patients had poor left ventricular contractility and were hemodynamically unstable. In each case, the device supported the failing circulation with blood flow rates and aortic pressures within acceptable ranges.

Patients supported with cardiovascular devices fabricated with smooth blood-contacting surfaces require the administration of large doses of anticoagulative and antiplatelet agents to minimize thrombogenesis and thromboembolic events [5]. In the present study, all 11 patients during LVAD support were administered relatively minimal antithrombotic therapy which has been modified and gradually reduced since clinical trials began in 1986. Patients were administered heparin alone for the durations of their pump support or heparin intraoperatively, followed by treatment with 10% low-molecular-weight dextran, and/or dipyridamole (75 mg/day)/low-dose aspirin (80 mg/day). After hemostasis was achieved, the prothrombin and partial thromboplastin times of all patients were within normal ranges. Despite minimal antithrombotic treatment, none of the patients experienced any device-related thromboembolic episodes.

Morphological and Ultrastructural Features of the Blood-Contacting Surfaces

Upon gross inspection after device removal, the blood-contacting surfaces of the diaphragms and opposing housings were covered with adherent, uniformly thin, glistening coatings. Both surfaces of the pumps appeared smooth and free of thrombus accumulation. There were, however, white, irregularly shaped islands of dense

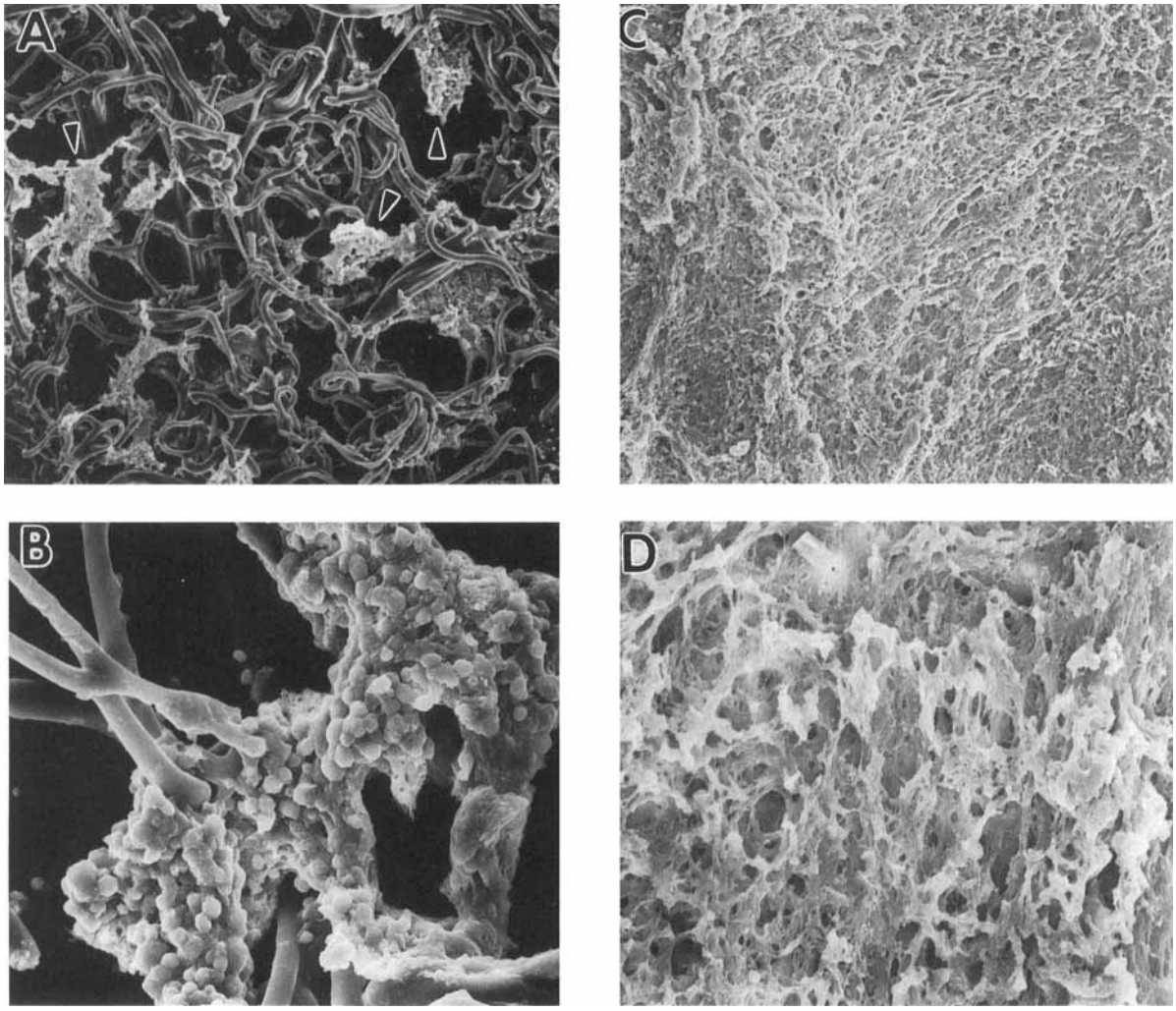

Fig. 4. Representative scanning electron photomicrographs of the diaphragm blood-contacting surface following 132 days of implantation. **A:** Relatively acellular region of the lining showing small aggregates (*arrows*) of dense cellular tissue attached to the integrally textured polyurethane fibrils (×100). **B:** High magnification of a tissue aggregate that developed around an individual fibril showing the cellularity of the deposit (×500). **C:** Compact fibrinous region of the lining. The polyurethane fibrils in this region are totally embedded beneath the lining (×100). **D:** Higher magnification of this region showing the porous nature of the matrix (500×).

fibrous tissue distributed over the housing surfaces retrieved from the 35-, 37-, 84-, 114-, 132-, 189-, and 324-day implants. White tissue islands were also observed on the diaphragm surfaces following 84, 114, 132, 233, and 324 days of implantation. The islands ranged in size from 0.1 to 3.0 cm in diameter. The number of deposits ranged from as few as 2 or 3 per device to as many as 23 per device (114-day implant). No pattern of deposition or preferential localization of the white tissue islands was evident among the explanted devices found to have these deposits. The number of islands per device did not correlate with length of implant duration.

As revealed by SEM, the biological linings that developed on the surfaces of these devices were heterogeneous with respect to morphology, tissue density and the degree of cellularity. As evaluated in cross section, the total thickness of the linings, even in the longer term implants, never exceeded 150 μm. The morphology of the linings did not significantly change beyond one month of implantation. Figure 4 illustrates the predominant surface morphology. A discontinuous layer of cells of various shapes inhabited the surfaces. Some regions of the linings, as shown in Figure 4A,B, were composed of periodic clusters of dense cellular tissue, which had accumu-

lated around the individual diaphragm fibrils, interspersed between relatively acellular areas. Other regions of the lining, however, were composed of fibrinous material which totally covered the fibrils (Fig. 4C,D). SEM of the scattered white islands observed on both the housing and diaphragm surfaces indicated a highly cellular surface. Some areas of the islands were covered with multiple rounded cells (Fig. 5A), while other areas were covered with what appeared to be highly flattened cells covered with matrix material (Fig. 5B). When viewed in cross section (Fig. 5C), the islands appeared laminated as though the biological lining had been deposited in layers. Little differences were observed in the morphology of the biological linings when samples that had been subjected to different combinations of flow/flex patterns were compared.

Histological evaluation of the resultant linings confirmed a laminated tissue organization and heterogeneity in the degree of tissue cellularity. The predominant lining morphology is represented in Figure 6A, which illustrates a largely organized fibrin matrix comprised of mononuclear cells of various shapes situated at both the blood-contacting surface and interspersed within the matrix. Within the tissue islands, layers of collagen were found interspersed between layers of a fibrinous matrix (Fig. 6B). Metachromatic staining with toluidine blue did not indicate a matrix with detectable glycosaminoglycan content (data not shown).

TEM of the white tissue islands also revealed a laminated tissue organization (Fig. 7). The blood-contacting surface of the islands were lined with a single layer of mononuclear cells (Fig. 7A). The middle layers of the deposit were composed of regions of loosely organized layers of fibrinous matrix containing large numbers of embedded cells (Fig. 7B). By contrast, the layer of tissue adjacent to the biomaterial interface was composed of an electron-dense amorphous material, sparsely populated with mononuclear cells (Fig. 7C). Other regions of the islands were composed of a highly collagenous matrix (Fig. 7D) interspersed with elongated fibroblastic-like cells. Many of these fibroblast-like cells contained microfilaments with associated dense bodies that encased the cell beneath the plasma membrane which distinguished them as myofibroblasts (Fig. 8). However, trichrome staining (Fig. 6B) of the tissue island did not reveal organized muscle fibers.

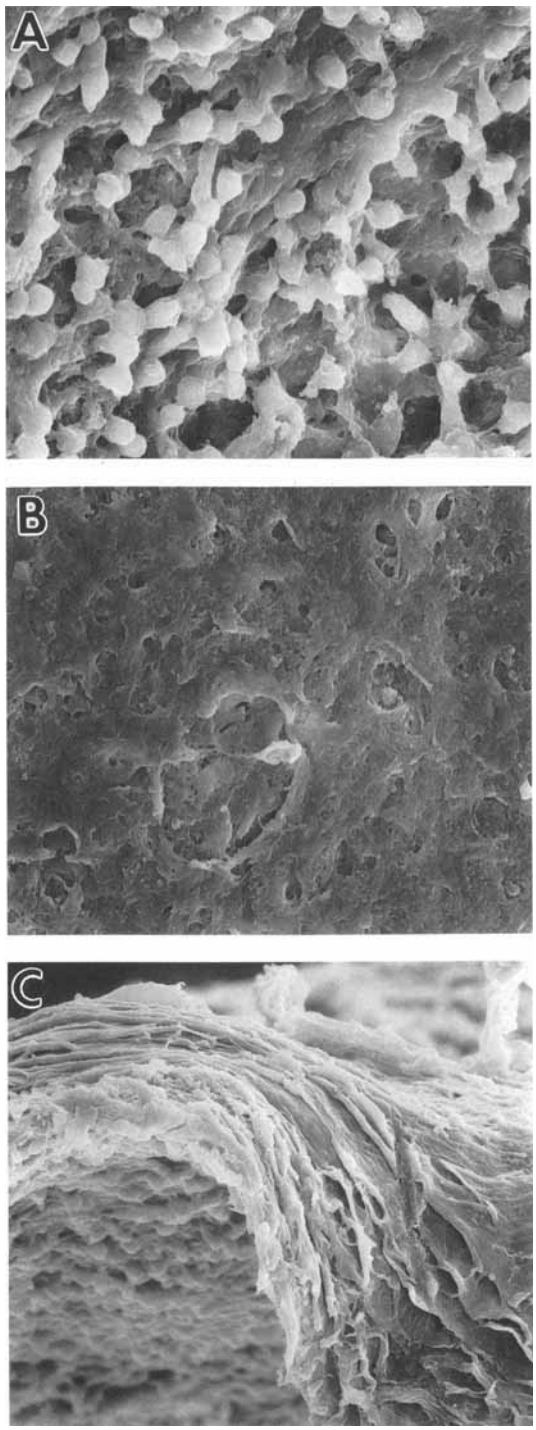

Fig. 5. Representative scanning electron photomicrographs showing the cellular blood-contacting surface of a typical "white" tissue island. **A:** Surface region composed of round-shaped cells (1,000×). **B:** Adjacent region comprised of highly flattened cells (×500). **C:** Cross-sectional view showing the laminated nature of the deposit (×500). The island was removed from the housing surface of the 132-day implant.

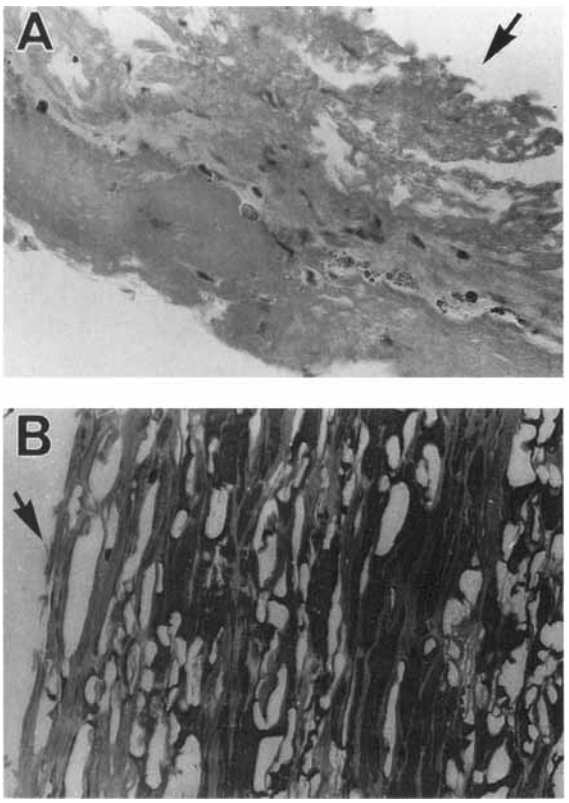

Fig. 6. Histological sections of the lining from the diaphragm surface of the 132-day implant. **A:** Representative full-thickness cross section showing the presence of mononucleated cells dispersed throughout the tissue. *Arrows,* blood-contacting lumenal surface. (Hematoxylin & eosin-stained, ×40.). **B:** Tissue island excised from the diaphragm demonstrating a largely collagenous matrix (pale-staining regions) with interspersed laminated fibrinous matrix (darker-staining regions). (Trichrome-stained, ×32.) The titanium housing tissue islands had a similar collagen/fibrin laminated morphology.

Biochemical Composition of the Neointimal Lining

To quantitate total collagen and protein accumulation on the LVAD blood contacting surfaces, tissue deposits on 1–2-cm^2-diaphragm samples, which had been exposed to different combinations of hemodynamic conditions and mechanical flexure patterns (Fig. 3), were subjected to amino acid analyses. As illustrated in Figure 9, the quantities of total protein deposited on the diaphragm samples were highly variable. Where two samples were available from the same region (e.g., 35-, 132-, and 189-day diaphragms), values ranged widely. Generally, protein content per cm^2 was greater in the high shear regions (Fig. 9A,B). In low-flex regions, no significant correlations as a function of implant duration were found with either high-shear (Fig. 9B, r = 0.048) or low-shear (Fig. 9C, r = 0.260) conditions. In high-flex regions, there were trends toward increased protein accumulation in the high-shear areas (Fig. 9A, r = 0.734) and a decrease in the low-shear regions (Fig. 9D, r = 0.523) as a function of increasing implant duration.

Collagen was only detected within the white tissue islands. The percent collagen of the total protein deposited in these islands ranged from 22% (132-day implant) to 37% (114-day implant). White islands removed from the housings of the 84- and 324-day implants were found to contain similar quantities of collagen (29% and 28%, respectively).

To detect for possible pathological calcification, representative samples from 7 pump diaphragms (35, 84, 114, 132, 189, 233, and 324 days) and 3 pump housings (132, 233, and 324 days) were subjected to energy dispersive X-ray spectroscopy (EDS). Special attention was given to samples removed from the flexing regions of the diaphragm which have been shown to be associated with a high incidence of calcification in bovine studies [26,27]. As shown in Figure 10, the major elements of the biological lining included carbon, oxygen, sodium, aluminum and sulfur. The elemental profiles of each sample did not significantly vary with respect to either the length of implant duration or flex/shear conditions. Calcific deposits were not detected in any of the samples evaluated.

Gene Expression of the Colonizing Cells

To characterize cellular growth properties and synthesized products of cells associated with the titanium and polyurethane surfaces, RNA was extracted from the tissue linings harvested from both the housing and diaphragm surfaces of the 84-, 132-, and 324-day implants and from the diaphragms of the 31-, 114-, and 189-day implants. For the polyurethane diaphragms, the tissue linings were harvested from one quarter of the total diaphragm (outflow quadrant), whereas linings were harvested from the entire housing surface. The total quantities of RNA extracted from these samples are shown in Table II. Total RNA yields obtained from the diaphragm quadrants ranged from 165 μg (114-day implant) to as high as 739 μg (84-day implant). RNA extractions from the linings on the 84-, 132-, and 324-day housing components resulted in total RNA yields of 323, 175, and 403 μg, respectively.

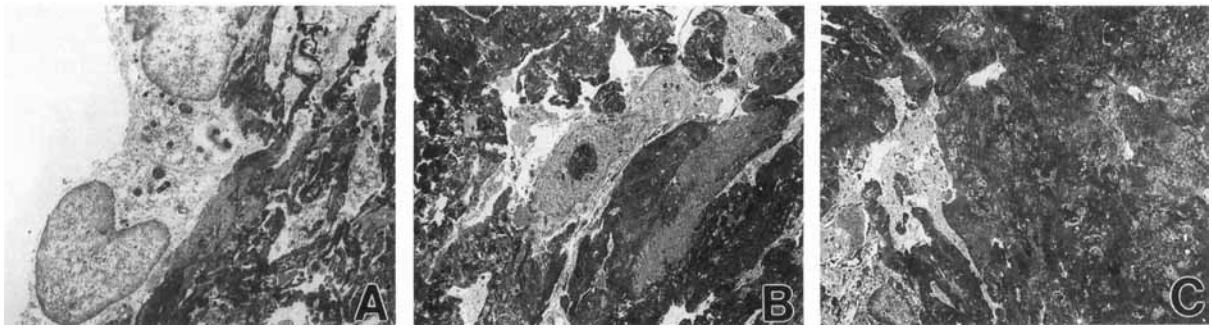

Fig. 7. *Transmission electron micrographs showing the ultrastructural features of a tissue island (from the polyurethane surface, 114-day explant). Full-thickness cross section of a noncollagenous region of the island (A–C).* **A:** *Lumenal surface of island demonstrating a layer of cells lining the blood–tissue interface (×3,500).* **B:** *Middle region of deposit showing a dense fibrinous matrix interspersed with numerous mononuclear cells (2,450×).* **C:** *Basal layer (i.e., region adjacent to the biomaterial interface) of tissue deposit showing a relatively acellular, highly compact matrix material (×2,450).* **D:** *High magnification (×26,250) of a collagenous region of the island illustrating a matrix composed largely of individual, loosely organized, collagen fibrils.*

The intactness of the isolated cellular RNA samples was quantitated by ethidium bromide staining following electrophoresis of the RNA on agarose gels. As indicated in Figure 11, differences were found in the integrities of the RNA samples, as reflected by the intactness of the 28S and 18S ribosomal RNA bands. The RNAs isolated from the linings on the diaphragm and housing surfaces of the 84- and 132-day implants, as well as from the diaphragm of the 31-day implant, were relatively intact. These 3 devices were removed from the patients immediately after the pneumatic drive consoles were turned off. However, the 28S and 18S ribosomal RNA bands of the diaphragm sample from the 189-day implant (device off for 3.5 h before actual retrieval) were less prominent, while the ribosomal RNA bands of the diaphragm sample from the 114-day implant (device off for 32.5 h before actual retrieval) were totally absent, indicating the RNA was extensively degraded. Although explantation of the 324-day implant was not staged, the integrity of the RNA isolated from the lining was similar to that of the 189 day implant and was apparently due to a delay in processing the pump components upon device removal.

The isolated RNA samples were subjected to hybridization analyses to determine if the cells colonizing the pump surfaces expressed genes encoding proteins for cell proliferation (histones), cell adhesion (fibronectin), cell shape (actin, vimentin), and extracellular matrix (collagen types I and III). RNA samples from each device were hybridized simultaneously to each cDNA probe to permit direct comparison of mRNA levels between samples. The RNA extracted from the diaphragm lining of the 114-day implant, which was found to be totally degraded, was not analyzed.

Relative levels of mRNA transcripts of cell growth-, cytoskeletal-, and extracellular matrix-related genes in cells colonizing the LVAD diaphragm surfaces as a function of implant duration are shown in Figure 12. Histone mRNA expression indicated that cellular proliferation occurred within the matrix. FN mRNA levels for the 31-, 84-, and 132-day samples were relatively high compared to the 189- and 324-day samples. The level of type III collagen mRNA was highest in the 31-day sample, whereas levels in the 84-, 132-, and 189-day samples were greatly reduced. By contrast, type I collagen mRNA expression was greatest in the 132 and 324 day implants, while expression in the other three implants, particularly at 31 and 189 days, was extremely low. The expression of mRNAs for the 2 cytoskeletal-associated genes followed similar patterns with respect to implant duration. Levels of both actin and vimentin mRNAs

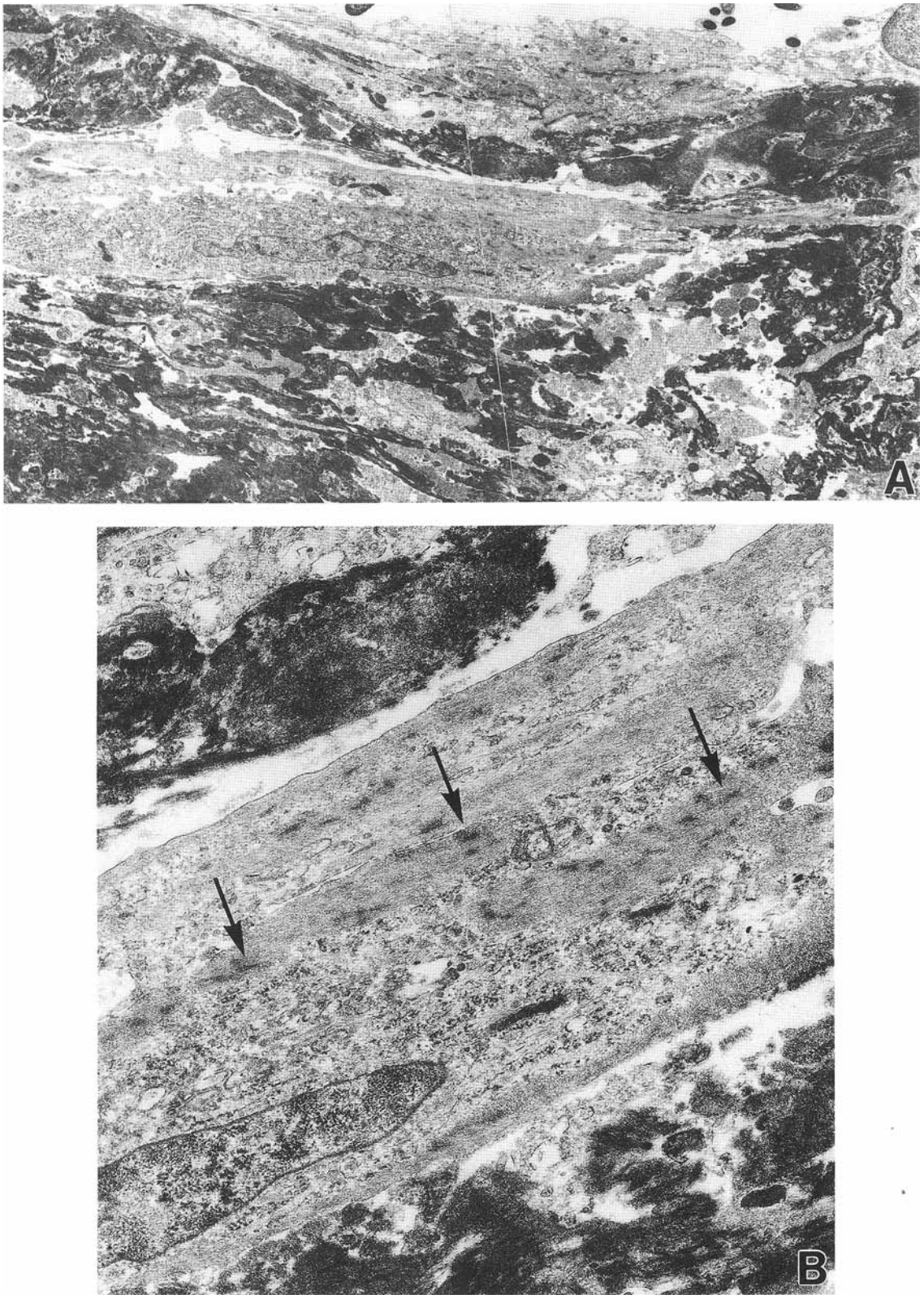

Fig. 8. Ultrastructural identification of myofibroblasts in a tissue island. **A:** Several elongated cells showing microfilaments with dense bodies in the cortex of the cell. (×5,750.) **B:** Higher magnification of the cortical region of the cell illustrating the presence of abundant microfilaments. *Arrows,* dense bodies. (×21,125). The sample was removed from the titanium housing surface of the 132-day explant.

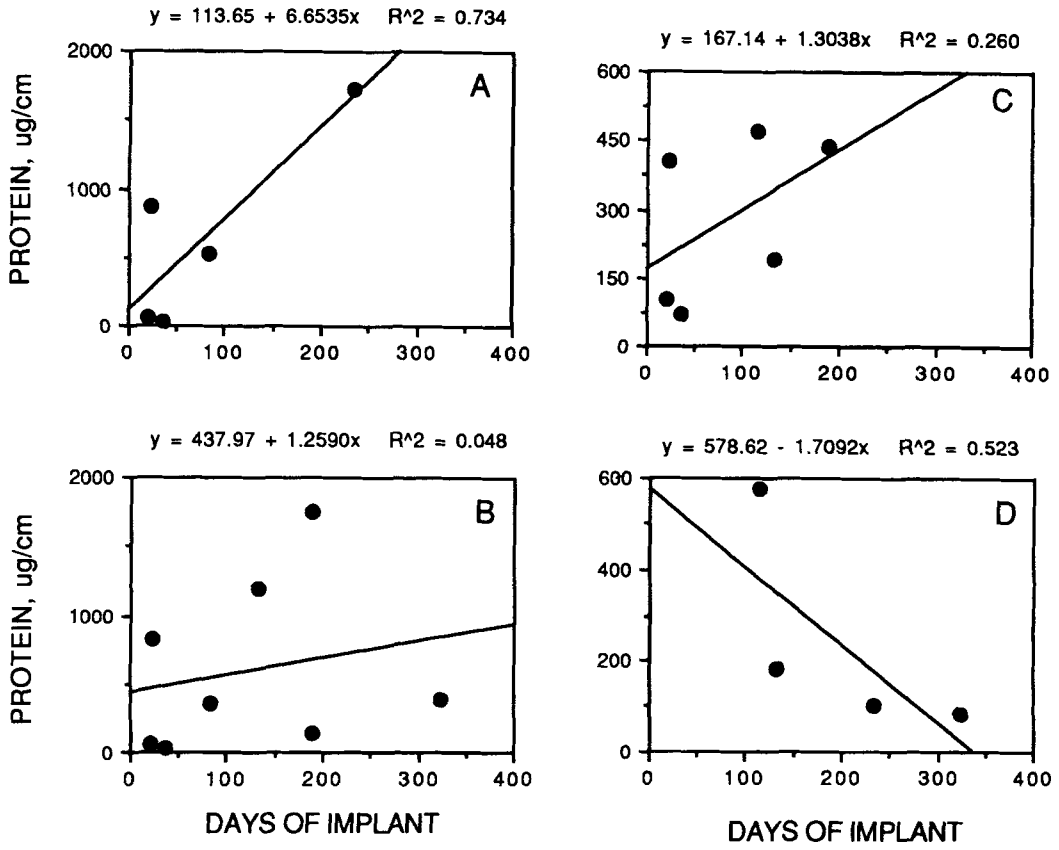

Fig. 9. Relationship of protein deposition to flex/shear conditions and implant duration. Tissue deposits on diaphragm samples exposed to various combinations of hemodynamic and mechanical flexure conditions were hydrolyzed and subjected to amino acid analysis as described. **A:** High shear/high flex. **B:** High shear/low flex. **C:** Low shear/low flex. **D:** Low shear/high flex (Fig. 3).

were virtually identical in the 31-, 84-, and 132-day implants, while at 189 and 324 days of implantation, levels were more than 50% lower.

Figure 13 illustrates the relative levels of gene expression by cells populating the housing surface as a function of implant duration. Fibronectin mRNA expression was highest at 132 days and lowest at 324 days of implantation. For type I collagen, mRNA levels were high in the 84 and 132 day implants compared to the 324-day implant, whereas levels of type III collagen mRNA were higher in the 132-day implant compared to the 84-day implant. Actin and vimentin mRNA levels were highest in the 84- and 324-day implants, respectively. Cells colonizing the housing surfaces also expressed histone mRNA.

DISCUSSION

The conventional approach in the development of long-term circulatory assist (left ventricular assist) and replacement (total artificial heart) devices has been to fabricate the blood-contacting surfaces from polyurethanes having a smooth topography [1,2]. The rationale is to create a nonthrombogenic surface which does not promote the accumulation of blood-derived deposits. However, despite improvements in biomaterials, the polyurethanes currently used in these devices (typically Biomer) still exhibit thrombogenic properties [3,4]. In addition, seams and junctions between device components, as well as microscopic surface imperfections that arise during fabrication, all serve as a potential nidus for thrombus formation. Consequently, devices fabricated with smooth blood-contacting surfaces, such as the Thoratec Pierce-Donachy prosthetic ventricle, the Novacor left ventricular assist system, and the Jarvik-7 total artificial heart, often develop focal, poorly adherent thrombi which have the potential for embolization [5–7]. An alternative approach for controlling thromboembolic events involves the use of textured biomaterials for the blood-contacting surfaces. In contrast to smooth surfaces, tex-

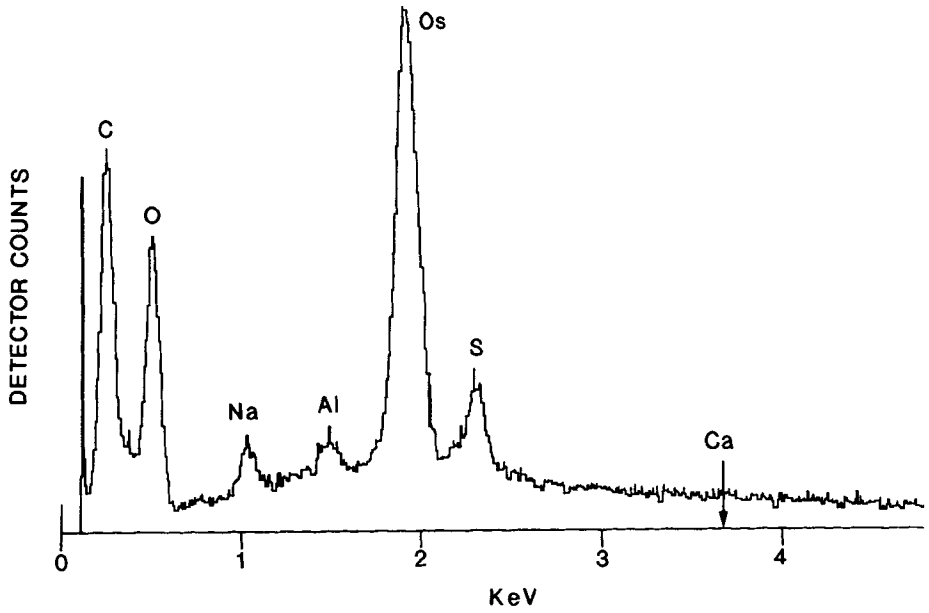

Fig. 10. Representative EDS analysis of the biological linings. The elemental composition of the linings included carbon (C), oxygen (O), sodium (Na), aluminum (Al), and sulfur (S). Calcium (Ca), which emits at 3.69 KeV (*arrow*), was not detected in any of the samples. The presence of osmium (Os) is due to the postfixation of the sample in osmium tetroxide. All samples analyzed were found to have similar elemental profiles.

TABLE II. Total RNA Yields Harvested from LVAD Cell Linings

Implant duration	Pump component[a]	Total RNA yield (μg)
31	Diaphragm	579
84	Diaphragm	739
	Housing	323
114[b]	Diaphragm	165
132	Diaphragm	304
	Housing	175
189[b]	Diaphragm	576
324	Diaphragm	302
	Housing	403

[a]Cell linings were harvested from the outflow quadrant of the diaphragms (i.e., high shear region) and from the entire surface of the housings.
[b]Staged explantations.

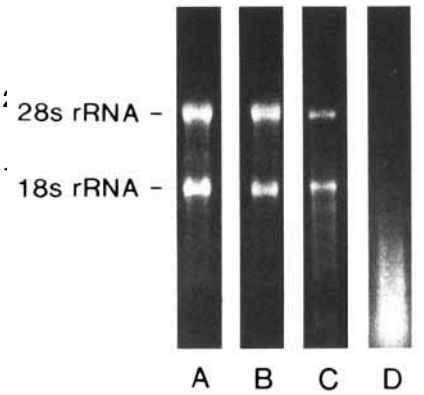

Fig. 11. Evaluation of cellular RNA integrity. Extracted RNA samples were stained with ethidium bromide following electrophoresis in 6.6% formaldehyde–1% agarose gels. Representative integrities of RNA isolated from the diaphragm (lane A) and housing (lane B) surfaces of an LVAD in which explantation was nonstaged (132-day implant). Note the intactness of the 28s and 18s ribosomal RNA bands. Lane C, Integrity of RNA isolated from a device explanted after a delay of 3.5 h. Lane D, RNA isolated from a device explanted after a delay of 32.5 h. Note the complete absence of the ribosomal RNA bands. Ten μg of RNA were loaded per lane.

tured blood-contacting surfaces are designed to encourage the formation and adherence of a biological pseudointimal lining derived from circulating blood elements. The resultant lining ultimately functions as the permanent, biocompatible blood-contacting surface.

In clinically implanted LVADs fabricated with textured blood-contacting surfaces, the events at the blood/biomaterial interface within the first week of implantation involve the deposition of a thin, uniform, loosely organized, but well adherent, fibrin-cellular coagulum consisting of entrapped blood elements [15]. Our evaluation of longer-term implants demonstrated that after approximately 1 month, patches of dense cellular tissue, intermingled with adjacent regions of compact matrix material, developed on

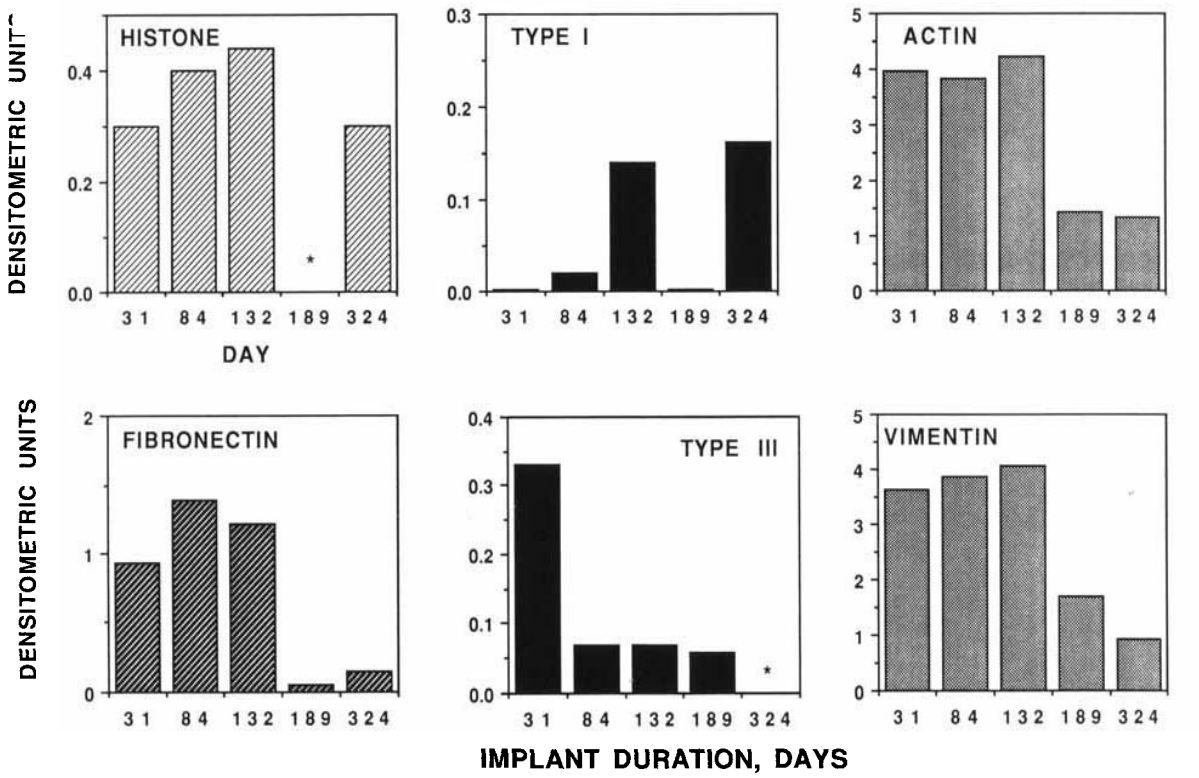

Fig. 12. Relative levels of gene expression by cells colonizing the diaphragm surface as a function of implant duration. Equal quantities of total cellular RNA from each sample were applied to Zeta-Probe membranes using a slot-blot apparatus (2 or 4 μg RNA/slot). The blots were then hybridized to gene-specific ^{32}P-labeled cDNA probes. Resultant autoradiograms were quantitated by scanning laser densitometry. Asterisks (*) indicate not analyzed.

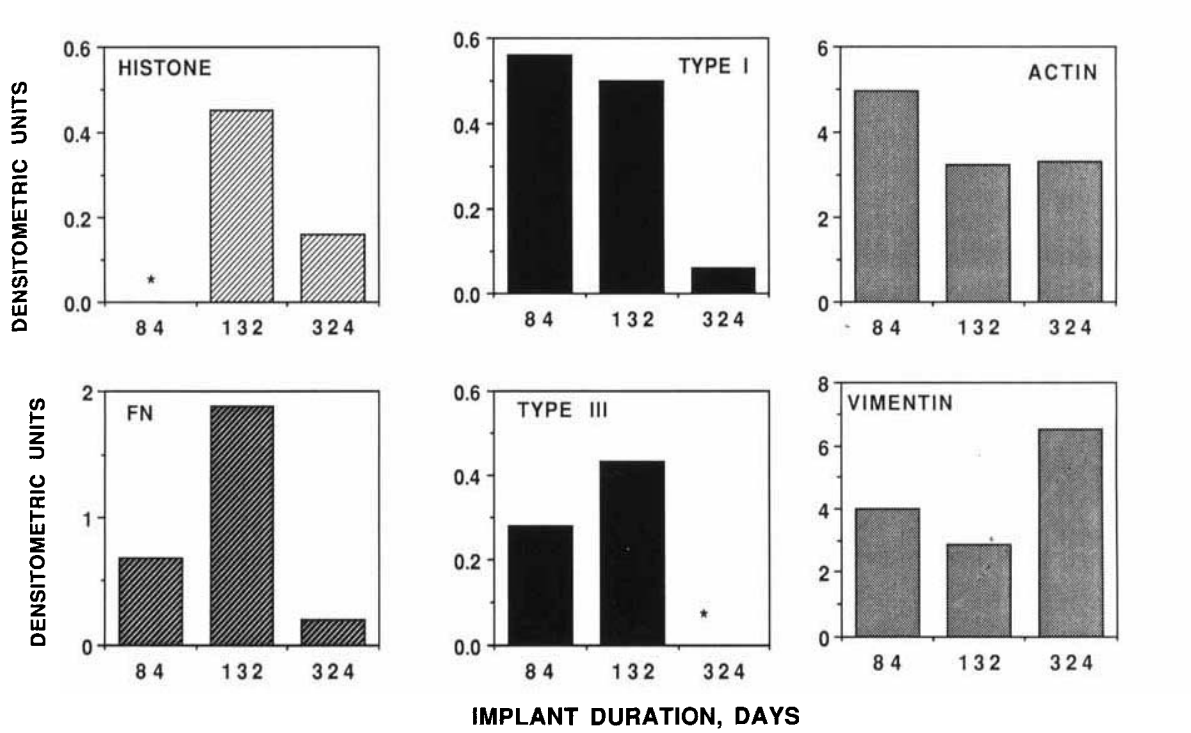

Fig. 13. Relative levels of mRNA transcripts in cells populating the housing surface as a function of implant duration. RNA samples were slotted, hybridized, and quantitated as described in Figure 12. Asterisks (*) indicate not analyzed.

the textured surfaces. Ultrastructural and histological evaluation revealed a laminated tissue organization. Both biochemical and ultrastructural analyses demonstrated the presence of collagenous regions predominantly localized within dense tissue deposits (i.e., white islands). These collagenous islands arose spontaneously at random locations on both the polyurethane and titanium blood-contacting surfaces and only appeared after greater than 30 days of implantation. The percentage of collagen comprising the tissue islands did not progressively increase as a function of implant duration.

To function successfully as a blood-contacting surface, a biological lining must exhibit hemocompatible properties, as well as remain tightly adherent to the underlying biomaterial surface in response to vigorous pulsatile flow conditions. The lining which developed on the polyurethane and titanium textured blood-contacting surfaces satisfied these important criteria. Even though minimal antithrombotic treatment was used, the housing and diaphragm surfaces of all of the pumps remained free of any gross (visible) thrombus accumulation. TEM and SEM analyses revealed that the fibrils and microspheres of the diaphragm and housing surfaces were deeply integrated within the deposited lining, forming a highly intimate biomaterial-tissue interface. Most importantly, none of the patients supported with this LVAD experienced any device-related thromboembolic events, further indicating the formation of a tightly adherent lining. Textured blood-contacting surfaces thus offer a major advantage over the conventional smooth blood-contacting surfaces where embolism of excess thrombus material compromises clinical efficacy.

A biological lining functioning as a blood-contacting surface must also remain viable over time, a property which becomes especially important during long-term implantation. Our findings suggest that the linings that developed on the LVAD blood-contacting surfaces remained viable after extended periods of implantation. Ultrastructural and histological evaluation revealed the presence of viable cells embedded within the layers of the tissue linings. In addition, the RNA hybridization analyses indicated that the colonizing cells remained metabolically active for almost one full year, proliferating and synthesizing a variety of cytoskeletal and extracellular matrix proteins. Several properties of the linings probably played an important role in maintaining cell viability. Because of the impermeable nature of the LVAD pump components, nourishment of the lining can only occur by diffusion of plasma substrates from the lumenal surface [28]. The resultant lining must therefore remain thin enough such that the diffusion path of nutrients from the lumen is not exceeded. The total thickness of the linings did not significantly increase beyond 1 month of implantation, never exceeding 150 μm, which thereby facilitated the diffusion of nutrients from the circulating blood. Furthermore, the open, porous topographical architecture of the lining, which consisted of numerous channels and voids that extended downward to the base of the polyurethane diaphragm, facilitated nourishment of cells situated within the deeper layers of the lining.

A primary indication of the loss of lining viability involves the development of calcified lesions [29,30]. Deposition of calcific deposits on the flexing surfaces of blood pumps limits their functional longevity. The rigid mineral deposits can result in the deterioration of pump performance through the loss of diaphragm compliance or the initiation of tears, or can become a site for thrombi formation, providing a source of emboli. The thickness of the lining is believed to be a major factor, since the calcification process always initiates within necrotic tissue situated within the deepest layers of the lining, at the biomaterial-pseudointimal interface, and not from the lumenal surface [26,30]. In a bovine calf model, the pseudointimas of flexing bladders having textured fibrillar surfaces have been reported to undergo extensive calcification within 130 days of implantation, reaching thicknesses of 2–8 mm [10]. Although preseeding the textured surfaces with fibroblasts prior to implantation resulted in the formation of a thinner lining, calcification still occurred [10]. By contrast, the linings that developed on the human LVAD surfaces remained free of pathological calcification after implantation for as long as 324 days. Even though there was an apparent trend toward increased protein deposition in high shear regions over time, the linings did not sufficiently increase to a thickness which initiated calcification. Reasons for differences in the development of the human and bovine linings remain unknown but may be related to species differences in blood physiology or to the accelerated growth characteristics of the bovine calf model [27].

The necessity of providing nourishment to the biological lining in maintaining cell viability is indicated by the integrities of the RNAs isolated from the 114- and 189-day LVADs. For surgical-related reasons, the drive consoles were turned off, the inflow conduits were clamped closed, and the LVADs were left remaining in the patients for a period of time before actual removal. During this interval, blood no longer circulated through the devices. The integrity of the total cellular RNA isolated from the LVAD linings directly reflected the length of time removal of the device was delayed. A delay of only 3.5 h significantly reduced the integrity of the RNA, whereas an explantation delay of over 30 h resulted in total RNA degradation, indicating extensive cell degeneration had occurred. Continuous blood perfusion through the device, which provides nutrients and oxygen, is therefore critical for sustaining the viability of the biological lining. This finding also emphasizes the fact that a device which has been turned off for any significant period of time should not be restarted because of the possibility of necrotic tissue detaching and embolizing upon the resumption of blood flow.

RNA hybridization analyses demonstrated that the cells colonizing the LVAD textured blood-contacting surfaces actively expressed genes encoding proteins for cell proliferation, cytoskeleton and extracellular matrix. Cells populating the housing and diaphragm surfaces of the 132- and 324-day implants expressed H_4 histone mRNA, indicating the cells on both surfaces were actively proliferating. Cells synthesized an abundance of actin and vimentin mRNA transcripts. These high levels of cytoskeletal gene expression indicate an extensively developed cytoarchitecture. Colonizing cells also synthesized an extracellular matrix composed of types I and III collagen as well as fibronectin, a molecule necessary in cellular adhesion to the substratum.

Ultrastructural analysis of the tissue islands revealed cells containing numerous microfilaments with dense bodies distributed beneath the plasma membrane. These ultrastructural features are characteristic of a myofibroblast cell type [31]. The finding of large quantities of actin and vimentin mRNAs, as well as type III collagen mRNA, is also consistent with the presence of myofibroblasts [31]. Myofibroblasts have also been identified in the pseudointima of vascular prostheses in dog [32] and sheep [33], as well as in the pseudointimal linings of LVADs implanted into calves [34]. However, the origin of this cell type in pseudointimal linings remains unknown. The impermeable walls of the LVAD eliminate the surrounding tissue as a possible source of cells capable of contributing to pseudointimal development. Moreover, the anastomoses, another potential source of cells, are remote from the chamber (20–30 cm), making it unlikely that the cells migrated to the pump surfaces within the short period of time in which they were typically seen. Therefore, the most likely source of these cells is from the circulating blood. The myofibroblasts may be derived from a blood-borne pluripotential stem cell released from the bone marrow. After colonizing the pump surfaces, these circulating stem cells may then proceed to differentiate into myofibroblasts in response to the rigorous, dynamic environment of flex/shear stresses encountered within the pumping chamber (see below). Experiments using cardiac assist devices and vascular prostheses with impermeable walls suggest the existence of circulating multipotential mononuclear cells that have the potential to differentiate into a variety of mesenchymal cell types [32–35].

Although only a limited number of implants have been examined thus far, our findings indicate that the levels of gene expression change as a function of implant duration. In the 31-day implant, the levels of type III collagen mRNA transcripts in cells colonizing the diaphragm surface are relatively high, while the levels of type I collagen mRNA are negligible. At longer periods of implant duration, the levels of type III collagen mRNA were relatively low, whereas levels of type I collagen mRNA, with the exception of the 189-day implant, were increased. The negligible amount of type I collagen detected on the 189-day diaphragm quadrant that was analyzed can be explained by the finding that no collagenous islands had developed within this region. During development, levels of type III collagen, which predominate in fetal tissues, gradually decline, while type I levels increase and eventually predominate [31,36]. This apparent increase in the type I:III ratio with implant duration may therefore represent the development of a more complex and mature level of tissue organization. The lower expression of actin and vimentin mRNAs observed in the longer term implants (189 and 324 days) compared to the shorter term implants is also consistent with a remodeling of the maturing extracellular

matrix. The extracellular matrix, via interactions with transmembrane proteins (integrins) and cytoskeletal elements, has been shown to cause nuclear alterations that directly influence gene expression [37].

The biomaterial surface (i.e., housing versus diaphragm) colonized by the cells was also found to influence gene expression, particularly of the extracellular matrix-related genes. For example, type I collagen mRNA levels synthesized by cells populating the housing surfaces of the 84- and 132-day implants were 28- and 3.6-fold greater, respectively, than mRNA levels synthesized by cells populating the corresponding diaphragm surfaces within the same implant. Similarly, type III collagen mRNA levels for the 84- and 132-day housing implants were 4- and 6.1-fold greater, respectively, than the levels for the corresponding diaphragm implants. These differences may be related to the fact that cells harvested from the outflow diaphragm quadrants were primarily exposed to high shear rates, as well as high flexure stresses, whereas cells harvested from the static housings were exposed to a variety of shear rates (both low and high) and no flexure stresses. This finding is not surprising since cytoskeletal architecture [38,39] and extracellular matrix production [40,41] are known to be modulated by exposure to shear forces and mechanical flexure stresses. Shear stress modulation of extracellular matrix production by the colonizing cells may also be responsible for the greater degree of protein deposition found in high shear regions of the device compared to low shear regions. Additionally, differences observed in gene expression between the cells populating the housing and diaphragm surfaces may be related to surface chemistry-related properties of the polyurethane and titanium biomaterials (e.g., critical surface tension) as well as surface topography (fibrils versus microspheres) which may directly influence blood fluid dynamics at the cell–biomaterial interface.

In conclusion, the present study represents the first application of molecular biological techniques to the analysis of blood-biomaterial interactions in mechanical circulatory support systems. We have demonstrated that intact total cellular RNA can be isolated from the biological linings that develop on the blood-contacting surfaces of cardiovascular assist devices. A quantitation of the cellular levels of mRNA transcripts for a variety of gene products can then be performed. The information obtained allows one to determine the properties of the colonizing cells, including cytoskeletal and extracellular matrix production, which may reflect in vivo conditions, permitting interpretations with respect to implant duration or possibly a patient's physiological condition. Future studies analyzing a broader spectrum of gene transcripts using currently available cloned gene probes should provide additional information regarding cellular phenotype as well as functional properties of the colonizing cells (e.g., production of growth factors and/or antithrombogenic agents). This information, in conjunction with clinical data of patient management, may be important in evaluating the clinical efficacy of cardiac assist devices used for long-term circulatory support.

ACKNOWLEDGMENTS

The authors acknowledge James Makeeff at Jeol (Peabody, MA) for his expert technical assistance in performing the EDS analyses. This work was supported in part by the National Heart, Lung, and Blood Institute grants HL 07720 and HL 32355.

REFERENCES

1. Pierce WS, Meyers JL, Donarchy JH, Rosenberg G, Landis DL, Prophet GA, Snyder AJ (1981): Approaches to the artificial heart. Surgery 90:137–148.
2. Oyer PE, Stinson EB, Portner PM, Ream AK, Shumway NE (1980): Development of a totally implantable, electrically-actuated left ventricular assist system. Am J Surg 140:17–26.
3. Lelah MD, Lambrecht LK, Young B, Cooper S (1983): Physiochemical characterization and in vivo blood tolerability of cast and extruded biomer. J Biomed Mater Res 17:1–22.
4. Szycher M, Griffin JC, Williams JL, McMenamy JP, Stagg D (1987): Blood compatible polyurethane elastomers. J Biomat Applic 2:290–313.
5. Didisheim P, Olsen DB, Farrar DJ, Portner PM, Griffith BP, Pennington DG, Joist JH, Schoen FJ, Gristina AG, Anderson JM (1989): Infections and thromboembolism with implantable cardiovascular devices. Trans Am Soc Artif Intern Organs 35:54–70.
6. Schoen FJ, Clagett GP, Hill JD, Chenoweth DE, Anderson JM, Eberhart RC (1987): The biocompatibility of artificial organs. Trans Am Soc Artif Intern Organs 33:824–833.
7. Ward RA, Wellhausen SR, Dobbins JJ, Johnson GS, DeVries WC (1987): Thromboembolic and infectious complications of total artificial heart implantation. Ann NY Acad Sci 516:638–650.
8. Bernhard WF, LaFarge CG, Robinson TC, Yun I, Shirahige K (1968): An improved blood pump interface for left ventricular bypass. Ann Surg 168:750–764.

9. Szycher M, Poirier V, Bernhard WF, Franzblau C, Haudenschild C, Toselli P (1980): Integrally textured polymeric surfaces for permanently implantable cardiac assist devices. Trans Am Soc Artif Intern Organs 25:493–499.
10. Bernhard WF, Colo NA, Wesolowski JS, Szycher M, Fishbein MC, Parkman R, Franzblau CC, Haudenschild CC (1980): Development of collagenous linings on impermeable prosthetic surfaces. J Thorac Cardiovasc Surg 79:552–564.
11. Szycher M, Poirier V, Franzblau C, Faris B, Snider R, Toselli P, Haudenschild CC, Bernhard WF (1981): Biochemical, histological, and ultrastructural assessments of pseudoneointimal linings derived from fibroblast-seeded integrally textured polymeric surfaces. J Biomed Mater Res 15:247–265.
12. Lian JB, Levy RJ, Bernhard W, Szycher M (1981): LVAD mineralization and gamma-carboxyglutamic acid containing proteins in normal and pathologically mineralized tissues. Trans Am Soc Artif Intern Organs 27:683–690.
13. Nose Y, Harasaki H, Murray J (1981): Mineralization of artificial surfaces that contact blood. Trans Am Soc Artif Intern Organs 27:714–719.
14. Turner SA, Milton LT, Poirier VL, Norman JC (1981): Sequential studies of pseudoneointimae within long-term THI E-Type ALVAD's: Thickness, calcification, and compositional analyses. Artif Organs 5:18–27.
15. Dasse KA, Chipman SD, Sherman CN, Levine AH, Frazier OH (1987): Clinical experience with textured blood contacting surfaces in ventricular assist devices. Trans Am Soc Artif Intern Organs 33:418–425.
16. Skinner RA (1987): Modified Osheroff-Ruffing: An improved trichrome procedure for glycol methacrylate. J Histotechnol 10:249–250.
17. Peterkofsky B, Diegelman RF (1971): Use of a mixture of proteinase-free collagenase for the specific assay of radioactive collagen in the presence of other proteins. Biochemistry 10:988–994.
18. Grimes S, Weisz-Carrington P, Daum H III, Smith J, Green L, Wright K, Stein G, Stein J (1987): A rat histone H_4 gene closely associated with the testis-specific H1t gene. Exp Cell Res 173:534–545.
19. Gunning P, Ponte P, Okayama H, Engel J, Blau H, Kedes L (1983): Isolation and characterization of full-length cDNA clones for human alpha-, beta-, and gamma-actin mRNA's: Skeletal but not cytoplasmic actins have an amino-terminal cysteine that is subsequently removed. Mol Cell Biol 3:787–795.
20. Ferrari S, Battini R, Kaczmarek L, Rittling S, Calabretta B, De Riel JK, Philiponis V, Wei J-F, Baserga R (1986): Coding sequence and growth regulation of the human vimentin gene. Mol Cell Biol 6:3614–3620.
21. Schwarzbauer JE, Tamkun JW, Lemischka IR, Hynes RO (1983): Three different fibronectin mRNAs arise by alternative splicing within the coding region. Cell 35: 421–431.
22. Genovese C, Rowe D, Kream B (1984): Construction of DNA sequences complementary to rat a1 and a2 collagen mRNA and their use in studying the regulation of type I collagen synthesis by 1,25-dihydroxyvitamin D. Biochem 23:6210–6216.
23. Stepp MA, Kindy M, Franzblau C, Sonenshein G (1983): Cloning of type III collagen and expression in aortic smooth muscle cells. Ann NY Acad Sci 460:510–513.
24. Feinberg AP, Vogelstein B (1983): A technique for radiolabeling DNA restriction endonuclease fragments to a high specific activity. Anal Biochem 132:6–13.
25. Maniatis T, Fritsch E, Sambrook J (1982): "Molecular Cloning: A Laboratory Manual." Cold Spring Harbor, NY: Cold Spring Harbor Laboratory Press, p 544.
26. Lian JB (1985): Factors contributing to intracavitary calcification. In Rubin RP, Weiss GP, Putney JW Jr (eds): "Calcium in Biological Systems." New York: Plenum, pp 633–643.
27. Coleman D (1981): Mineralization of blood pump bladders. Trans Am Soc Artif Intern Organs 27:708–713.
28. Liotta D, Hall CW, DeBakey NE (1966): A permanent autologous lining for implantable blood pumps. Cardiovasc Res Bull 4:69–75.
29. Schoen FJ, Harasaki H, Kim KM, Anderson HC, Levy RJ (1988): Biomaterial-associated calcification: Pathology, mechanisms, and strategies for prevention. J Biomed Mater Res 22:11–36.
30. Levy RJ, Schoen FJ, Anderson HC, Harasaki H, Koch TH, Brown W, Lian JB, Cumming R, Gavin JB (1991): Cardiovascular implant calcification: A survey and update. Biomaterials 12:707–714.
31. Gabbiani G, Le Lous M, Bailey AJ, Bazin S, Delaunay A (1976): Collagen and myofibroblasts of granulation tissue. A chemical, ultrastructural and immunologic study. Virchows Arch B Cell Pathol 21:133–145.
32. Sottiurai VS, Batson RC (1983): Role of myofibroblasts in pseudointima formation. Surgery 94:792–801.
33. Feigl W, Susani M, Ulrich W, Matejka M, Losert U, Sinzinger H (1985): Organization of experimental thrombosis by blood cells. Evidence of the transformation of mononuclear cells into myofibroblasts and endothelial cells. Virchows Arch A Pathol Anat Histopathol 406:133–148.
34. Bossart MI, Turner SA, Milam JD, Connor DJ, Urrutia CO, Frazier OH (1982): Multipotential cells in the circulating blood: Ultrastructural evidence in the calf. Trans Am Soc Artif Intern Organs 28:185–189.
35. Mackenzie JR, Hackett M, Topuzlu C, Tibbs DJ (1968): Origin of arterial prosthesis lining from circulating blood cells. Arch Surg 97:879–885.
36. Fessler JH, Fessler LI (1978): Biosynthesis of procollagen. Annu Rev Biochem 47:129–162.
37. Bissel MJ, Aggeler J (1987): Dynamic reciprocity: how do extracellular matrix and hormones direct gene expression? In Cabot MC, McKeehan WL (eds): "Mechanisms of Signal Transduction by Hormones and Growth Factors. New York: Alan R. Liss, pp 251–262.
38. Ives CL, Eskin SG, McIntire LV (1986): Mechanical effects on endothelial cell morphology: in vitro assessment. In Vitro Cell Dev Biol 22:500–507.
39. Sumpio BE, Banes AJ, Buckley M, Johnson G Jr (1988): Alterations in aortic endothelial cell morphology and cytoskeletal protein synthesis during cyclic tensional deformation. J Vasc Surg 7:130–138.
40. Sumpio BE, Banes AJ, Link GW, Iba T (1990): Modulation of endothelial cell phenotype by cyclic stretch: Inhibition of collagen production. J Surg Res 48:415–420.
41. Sumpio BE, Banes AJ, Link WG, Johnson G Jr (1988): Enhanced collagen production by smooth muscle cells during repetitive mechanical stretching. Arch Surg 123: 1233–1236.